

AD-A070 796

AIR FORCE ROCKET PROPULSION LAB EDWARDS AFB CA
X-RAY SPECTROSCOPY AS A DIAGNOSTIC TOOL IN SOLID PROPELLANT COM--ETC(U)
MAY 79 W K MCGREGOR
AFRPL-TR-78-61

F/G 21/2

UNCLASSIFIED

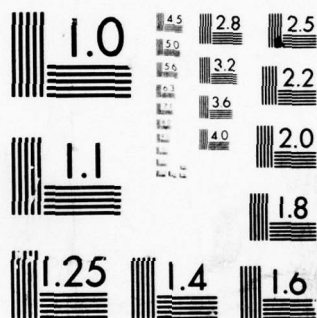
NL

| OF |
AD
A070796



END
DATE
FILMED

8--79
DDC



MICROCOPY RESOLUTION TEST CHART
NATIONAL BUREAU OF STANDARDS-1963-A

2 LEVEL

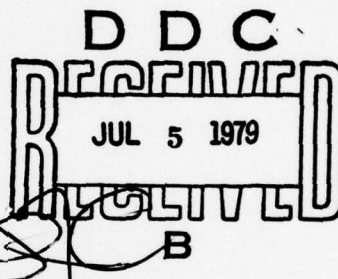
AFRPL-TR-78-61

X-RAY SPECTROSCOPY AS A DIAGNOSTIC TOOL IN SOLID
PROPELLANT COMBUSTION FLOWS

SPECIAL TECHNICAL REPORT - FEB 77 TO FEB 78

AIR FORCE ROCKET PROPULSION LABORATORY
EDWARDS AFB, CALIFORNIA 93523

AUTHOR: W. K. MCGREGOR



MAY 1979

Approved for public release;
Distribution Unlimited

DDC FILE COPY

AIR FORCE ROCKET PROPULSION LABORATORY
DIRECTOR OF SCIENCE AND TECHNOLOGY
AIR FORCE SYSTEMS COMMAND
EDWARDS AFB, CALIFORNIA 93523

79 07 03 021

NOTICES

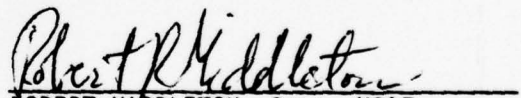
"When U.S. Government drawings, specifications, or other data are used for any purpose other than a definitely related government procurement operation, the Government thereby incurs no responsibility nor any obligation whatsoever, and the fact that the Government may have formulated, furnished, or in any way supplied the said drawings, specifications or other data, is not to be regarded by implication or otherwise, or in any manner licensing the holder or any other person or corporation, or conveying any rights or permission to manufacture, use or sell any patented invention that may in any way be related thereto."

FOREWORD

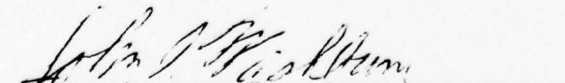
This work was performed in-house at the AFRPL under project number 2308M2UC, Combustion/Plume Diagnostics--Advanced Techniques. The author was on a temporary appointment to the AFRPL while on leave-of-absence from SVERDRUP/ARO, Inc., contract operator of the AFSC's Arnold Engineering Development Center. The author wishes to express his appreciation to the AFRPL for the opportunity to conduct the study reported herein and to acknowledge the many constructive discussions with his colleague, Dr. David M. Mann, which contributed materially to this report.

This report has been reviewed by the Information Office/XOJ and is releasable to the National Technical Information Service (NTIS). At NTIS it will be available to the general public, including foreign nations. This technical report has been reviewed and is approved for publication; it is unclassified and suitable for general public release.


DAVID M. MANN
Project Mgr. Plume Technology Section


ROBERT MIDDLETON, Capt, USAF
Chief, Combustion and Plumes Branch

FOR THE COMMANDER


JOHN I. WASHBURN, Lt Col, USAF
Chief, Propulsion Analysis Division

UNCLASSIFIED

SECURITY CLASSIFICATION OF THIS PAGE (When Data Entered)

REPORT DOCUMENTATION PAGE		READ INSTRUCTIONS BEFORE COMPLETING FORM
1. REPORT NUMBER 14 AFRPL-TR-78-61	2. GOVT ACCESSION NO.	3. RECIPIENT'S CATALOG NUMBER 9
4. TITLE (and Subtitle) 6 X-RAY SPECTROSCOPY AS A DIAGNOSTIC TOOL IN SOLID PROPELLANT COMBUSTION FLOWS.		5. TYPE OF REPORT & PERIOD COVERED Special Technical Report, Feb 77 to Feb 78
7. AUTHOR(s) 10 W. K. McGregor		6. PERFORMING ORG. REPORT NUMBER
9. PERFORMING ORGANIZATION NAME AND ADDRESS Air Force Rocket Propulsion Laboratory/PACP Edwards AFB, CA 93523		8. CONTRACT OR GRANT NUMBER(s)
11. CONTROLLING OFFICE NAME AND ADDRESS Air Force Rocket Propulsion Laboratory/PACP Edwards AFB, CA 93523		10. PROGRAM ELEMENT, PROJECT, TASK AREA & WORK UNIT NUMBERS 16 2308 M2UC 17 M2
14. MONITORING AGENCY NAME & ADDRESS (if different from Controlling Office) 1249p.		13. REPORT DATE 11 May 79
		15. SECURITY CLASS. (of this report) Unclassified
		15a. DECLASSIFICATION/DOWNGRADING SCHEDULE
16. DISTRIBUTION STATEMENT (of this Report) Approved for public release; distribution unlimited.		
17. DISTRIBUTION STATEMENT (of the abstract entered in Block 20, if different from Report)		
18. SUPPLEMENTARY NOTES		
19. KEY WORDS (Continue on reverse side if necessary and identify by block number) diagnostics rocket propulsion X-ray spectroscopy species measurement combustion		
20. ABSTRACT (Continue on reverse side if necessary and identify by block number) X-ray spectroscopy offers a potential method for the measurement of composition, elemental density, and particle mass in the gas/particle flows of solid propellant rockets. A theoretical analysis was performed from which it was concluded that both transmittance and fluorescence measurements in the 1 to 10 keV photon energy range will yield elemental densities of Al and Cl and transmittance can possibly give O, N and C densities, although sensitivity for the latter three elements to transmittance is poor. The sensitivity of		

DD FORM 1 JAN 73 1473

EDITION OF 1 NOV 65 IS OBSOLETE

UNCLASSIFIED

SECURITY CLASSIFICATION OF THIS PAGE (When Data Entered)

307 720

79 07 03 02

UNCLASSIFIED

SECURITY CLASSIFICATION OF THIS PAGE(When Data Entered)

Block 20 (con't)

alpha → the K_{α} fluorescence measurement to Al and Cl density changes is much greater than the sensitivity of transmittance measurements. However, the latter are required in order to determine densities directly from fluorescence rates. Hence, a combined transmittance and fluorescence measurement system is warranted. An investigation of commercially available hardware indicated that adequate detection systems exist, but insufficient data on photon flux rates from typical X-ray generating tubes was available to assess the adequacy of X-ray beam sources. Recommendations for proof-of-principle experiments are made, and a rocket test scenario is described for application to solution of the two-phase flow loss problem in solid propellant rockets. ↑

UNCLASSIFIED

SECURITY CLASSIFICATION OF THIS PAGE(When Data Entered)

TABLE OF CONTENTS

<u>PARAGRAPH</u>	<u>TITLE</u>	<u>PAGE</u>
1.	Introduction.	3
2.	Theoretical Considerations.	6
2.1	Fundamental Processes	6
2.2	Application	11
2.2.1	Absorption.	13
2.2.2	Mean Fluorescence	22
2.2.3	Particle Fluorescence	25
3.	Implementation Considerations	29
3.1	System Description.	29
3.2	System Performance Criteria	35
4.	Discussion.	37
4.1	Laboratory Demonstration Experiments.	37
4.2	Concept of a Typical Rocket Test Application	37
4.3	Future Directions	41
5.	Conclusions and Recommendations	43
5.1	Conclusions	43
5.2	Recommendations	44
	References.	45

Accession For	
NTIS GRA&I	<input checked="checked" type="checkbox"/>
DDC TAB	<input type="checkbox"/>
Unannounced	<input type="checkbox"/>
Justification	
By	
Distribution/	
Availability Codes	
Dist	Avail and/or special
A	

LIST OF ILLUSTRATIONS

<u>FIGURE</u>	<u>TITLE</u>	<u>PAGE</u>
1	Illustration of Scattering, Absorption, and Fluorescence in X-Ray Spectroscopy	7
2	X-Ray Absorption Cross Section for Lead ($Z = 82$)	9
3	Orientation of X-Ray Absorption Path with Combustion Medium. . .	14
4.	X-Ray Absorption Cross Section Data for Species of Interest in Solid Propellant Rocket Exhausts	17
5a.	Matrix Equation for X-Ray Transmittance at Five X-Ray Energies Through Typical Solid Propellant Rocket Exhaust-Forward Matrix Equation	18
5b.	Matrix Equation for X-Ray Transmittance at Five X-Ray Energies Through Typical Solid Propellant Rocket Exhaust-Inverse Matrix Equation	19
6.	X-Ray Transmittance Array for Species of Interest in Solid Propellant Rocket Exhausts at Five Values of Energy	21
7.	Concept of X-Ray Fluorescence Measurements for Combustion Flow Diagnostics.	23
8.	Scattering Event Chronology for a Particle Passing Through an X-Ray Beam	27
9.	Schematic of X-Ray Beam Source	30
10.	Approximate X-Ray Energy Spectrum from Chromium Target	31
11.	Functional Diagram of Energy Dispersive X-Ray Detection System .	33
12.	Detector and Electronic Contributions to System Resolution . . .	34
13.	Concept of X-Ray Measurement of Elemental Concentration at Exhaust Plane of Solid Propellant Rocket Motors.	40

LIST OF TABLES

<u>TABLE</u>	<u>TITLE</u>	<u>PAGE</u>
1.	Mole Fraction of Nozzle Exhaust Products for Typical Aluminized Solid Propellant ($p = 1 \text{ atm}$, $T = 1291^\circ\text{K}$)	12
2.	Atomic Species Densities and X-Ray Properties for Species Contained in Typical Aluminized Propellant Rocket Exhaust	16

1. INTRODUCTION.

The development of higher performance solid propellant rocket motors requires in situ measurement of the spatially distributed properties of the gas/particle flow produced by the combustion process. Furthermore, the prediction of exhaust plume observables (infrared and ultraviolet emission signatures and visible exhaust trails produced by scattering of solar radiation off primary particles in the near field, or condensed aerosols in the far field) depends upon the properties of the gas and particle flow and their distribution in the flow field. Such properties include gas density, temperature and species concentration, particle composition and physical state, particle size, mass and velocity distribution, and particle temperature. The high temperature gas/particle flows produced in typical aluminized solid propellant rocket motors contain mostly H_2 , CO , HCl , H_2O , and N_2 gases, and liquid and/or solid particulate Al_2O_3 . Other metal additives produce, in kind, oxides and carbides. Thus, the measurement problem is concerned with determination of one or more of the gaseous species concentrations together with the gas temperature and, independently, the properties of the particulates such as Al_2O_3 .

Techniques which have been used for in situ measurements of properties of combustion flows include emission/absorption spectroscopy, Raman and fluorescent scattering for gas phase temperature and species concentration, and various Mie scattering techniques for particle velocity and size distribution measurements. Discussions of these techniques and their application appear in several review papers,¹⁻³ and a compilation of papers is given in a recent book.⁴

1. Goulard, R., Mellor, A. M., and Bilger, R. W., "Combustion Measurements in Air Breathing Propulsion Engines. Survey and Research Needs," Combustion Science and Technology, Vol. 14, 1976, pp. 195-219.

2. Self, S. A. and Kruger, C. H. "Diagnostic Methods in Combustion MHD Flows," Journal of Energy, Vol. 1, 1977, pp. 25-43.

3. "Applications of Non-Intrusive Instrumentation in Fluid Flow Research," AGARD CP-193, May 1976.

4. Zinn, B. T., Ed., "Experimental Diagnostics in Gas Phase Combustion Systems," Progress in Astronautics and Aeronautics, Vol. 53, AIAA Press, 1977.

Applications reported in the literature have been limited to laboratory flames or pure gaseous flows with little attention to the gas/particle flows of solid propellant rockets. In a recent assessment of the combustion flow measurement requirements for rocket propulsion and the techniques available to make the measurements,⁵ it was concluded that adequate techniques exist (in principle) for pure gas phase property measurements and for two-phase flows when particle loading is very small and that particle velocity and size measurements are possible in two-phase flows for a limited velocity, size distribution, and particle number density range. Unfortunately, existing gas-phase diagnostic techniques are limited to flows with small particle loading, and existing particle diagnostic techniques are limited to flows with particle sizes greater than about 0.2 μm , velocities less than about 1.5 km/sec, and solid mass loadings less than about 10 percent. These limitations preclude application of existing techniques to most solid propellant combustion phenomena. Furthermore, light scattering techniques (since they depend primarily upon the polarizability properties of the particle) can only address particle size and velocity and cannot provide information on composition, mass, or temperature.

A method to measure composition and mass must be based upon a physical principle that is element- and mass-dependent. The immediately obvious physical principle is the absorption and scattering of X-rays by atomic elements. X-ray energy spectroscopy, in which the spectral distribution of the fluorescence induced by an incident X-ray beam is measured, is a commonly used analytical tool for solid materials.⁶ Recently, Chun has reported on an X-ray absorption system used successfully to measure the concentration of

5. McGregor, W. K., "Assessment of In Situ Diagnostics for Application to Rocket Propulsion Problems," AFRPL-TR-78-62, (to be published).

6. Bertin, E. P., Principles and Practices of X-Ray Spectrometric Analysis, Plenum Press, New York, 1971.

iron particles suspended in a gas flow.⁷ Although the system used by Chun is not directly applicable to the measurement of aluminum concentration in rocket exhausts, the apparent success of that application provided impetus to the feasibility study described herein.

The subsequent sections of this report contain a description of the principles involved in application of X-ray absorption and fluorescence spectroscopy to gas/particle flows and the results of calculations aimed at determining whether the technique would be feasible as a diagnostic for solid propellant rocket motor combustion flows. The results of the feasibility study indicate that X-ray spectroscopy can be a very useful means of extracting information on the spatial distribution of elemental species in a gas/particle flow field. Consequently, a program of laboratory investigation is outlined leading to demonstration of the techniques involved and development of a methodology for making the measurements and interpreting them in terms of flow properties.

7. Chun, J. W., "Quantitative Measurement of Aerosol Particulates with an Energy Dispersive X-Ray Spectrometer," NWC-TP-6012, Naval Weapons Center, China Lake, CA, (to be published).

2. THEORETICAL CONSIDERATIONS.

2.1 Fundamental Processes.

In this section we give an elementary description of the X-ray interaction process using the classical shell model of the atom. More thorough treatments may be found in textbooks on the subject.⁶

The interaction of X-ray electromagnetic radiation with matter is mainly through energy exchange with the bound electrons of atoms. Figure 1 illustrates the interaction; electrons may produce either scattering of an incident X-ray photon or total absorption of the photon with the photon energy going into the ejection of the electron from the atom, thus ionizing it. The scattering may be elastic with only a change in momentum of the electron and photon and no change in the frequency of the X-ray photon; this is commonly referred to as Rayleigh scattering in which the photon energy is less than the binding energy of the electron. Or the scattering event may be inelastic with a change in energy state of the electron and a corresponding change in frequency of the X-ray photon; this is commonly referred to as Compton scattering in which the photon energy is greater than the energy of the bound electron. The Compton process competes with the absorption process, either producing excitation of the atom or ionization at the ionization potential. Because of the Pauli Exclusion Principle, inner shell electrons undergoing interaction with the X-ray photons (either Compton scattering or absorption) must either be expelled from the atom completely or be excited to a state in the outermost shell. Thus, a minimum amount of photon energy equal to the potential energy of the electron is required to eject the electron. For the low Z elements at incident photon energies near the ejection energy of the electron, the absorption of the photon is a much more efficient mechanism than Compton scattering for removing X-rays from the beam and provides the main component of the total absorption cross section.⁷

Subsequent to the absorption event, because the configuration with a missing inner shell electron is unstable, an outer shell electron falls into the inner shell with an accompanying emission of X-ray radiation. This radiation is

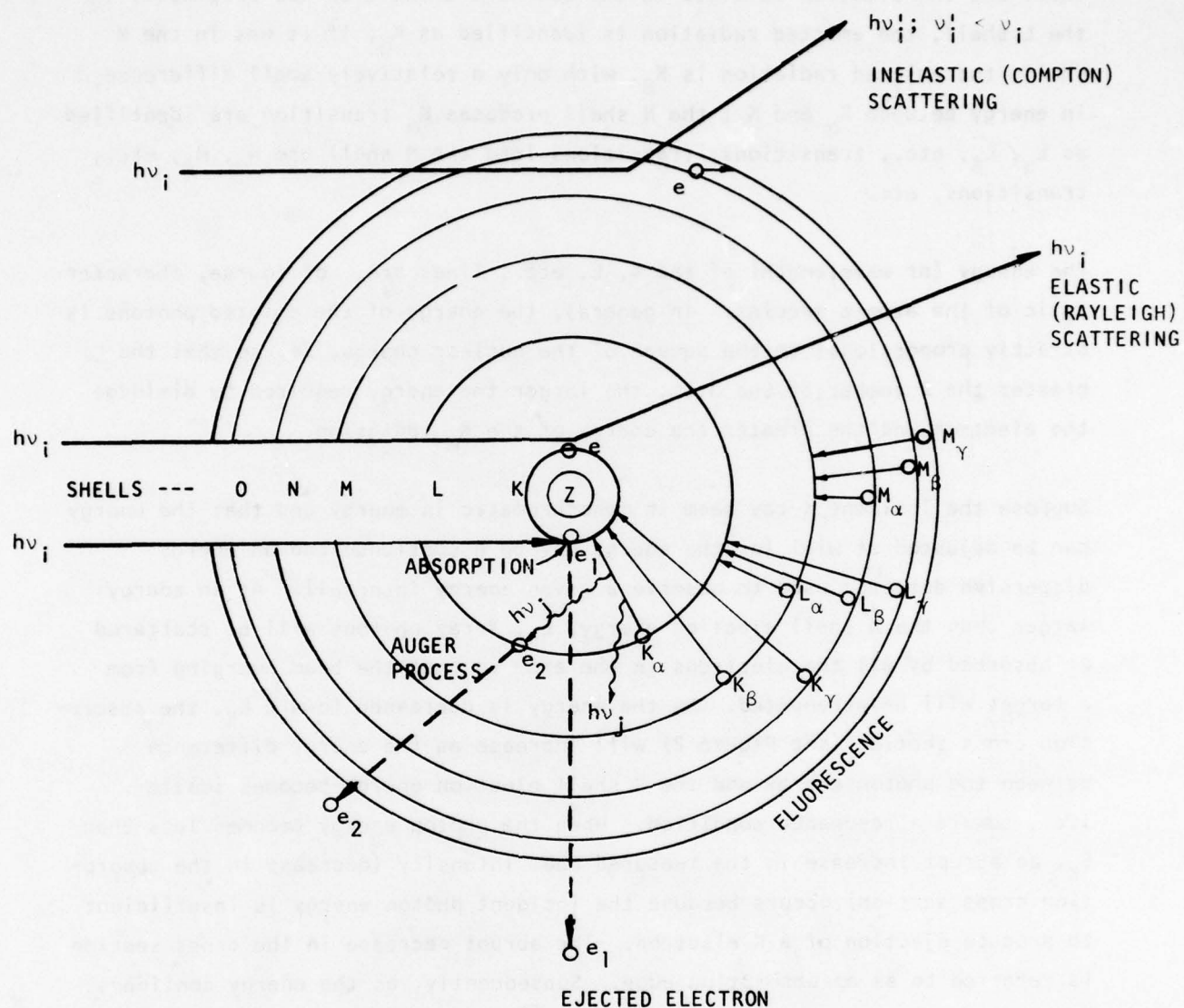


Figure 1. Illustration of Scattering, Absorption, and Fluorescence in X-Ray Spectroscopy.

known as X-ray fluorescence. If the ejected electron was in the innermost K shell and the electron involved in the downward transition was originally in the L shell, the emitted radiation is identified as K_α ; if it was in the M shell, the emitted radiation is K_β , with only a relatively small difference in energy between K_α and K_β ; the N shell produces K_α transition are identified as L_α , L_β , etc., transitions; transitions into the M shell are M_α , M_β , etc., transitions, etc.

The energy (or wavelength) of the K, L, etc., lines are, of course, characteristic of the atomic species. In general, the energy of the emitted photons is directly proportional to the square of the nuclear charge, Ze , so that the greater the Z number of the atom, the larger the energy required to dislodge the electron and the greater the energy of the K_α radiation.

Suppose the incident X-ray beam is monochromatic in energy and that the energy can be adjusted at will (or the energy may be a continuum and an energy dispersive detector used to observe a given energy interval). At an energy larger than the K shell ejection energy, E_K , X-ray photons will be scattered or absorbed by all the electrons in the atom so that the beam emerging from a target will be attenuated. As the energy is decreased toward E_K , the absorption cross section (see Figure 2) will increase as the energy difference between the photon energy and the K shell ejection energy becomes smaller, i.e., toward a resonance condition. When the photon energy becomes less than E_K , an abrupt increase in the measured beam intensity (decrease in the absorption cross section) occurs because the incident photon energy is insufficient to produce ejection of a K electron. The abrupt decrease in the cross section is referred to as an absorption edge. Subsequently, as the energy continues to be reduced, the absorption increases as before until the ejection energy of a second inner shell (L shell) is reached, where a second abrupt decrease in absorption is observed. As the energy is decreased further, the absorption continues to increase because of interaction with outer shell electrons. This process is illustrated in Figure 2 where the absorption cross section of lead (Pb, $Z = 82$) is shown. The cross section σ_α is found by experiment to be approximately of the form⁶

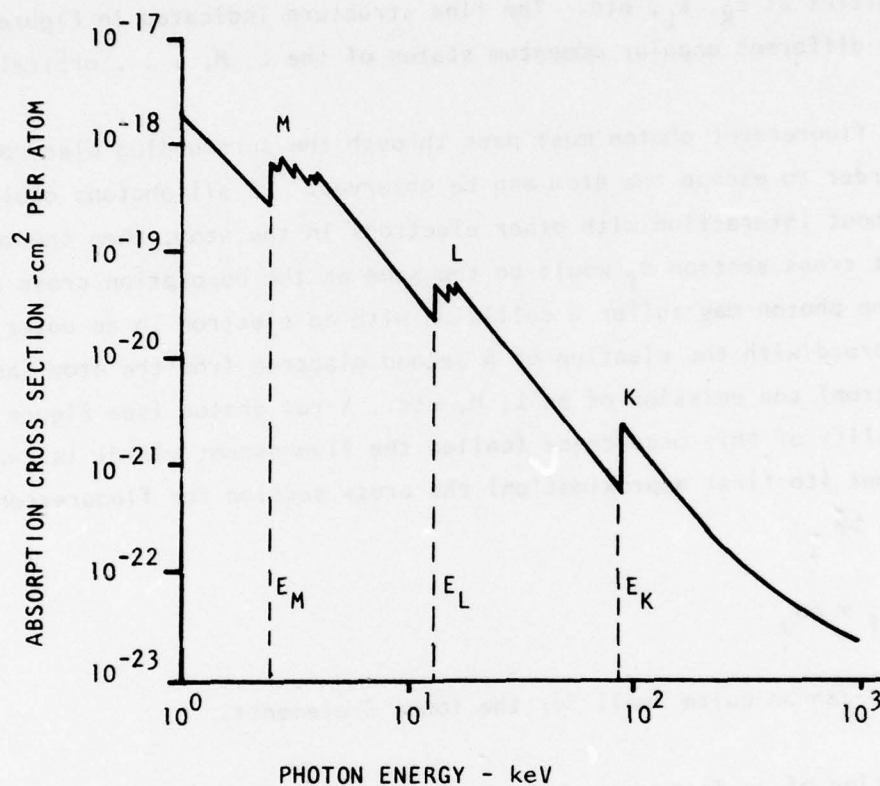


Figure 2. X-Ray Absorption Cross Section for Lead ($Z = 82$).

$$\sigma_{\alpha} = C Z^4 E^{-3} + b \quad (1)$$

except for the characteristic jumps, where E is the photon energy, Z is the atomic number, and C and b are constants which are different between the discontinuities at E_K , E_L , etc. The fine structure indicated in Figure 2 is due to the different angular momentum states of the L , M , . . . orbitals.

An emitted fluorescent photon must pass through the surrounding electron cloud in order to escape the atom and be observed. If all photons could escape without interaction with other electrons in the atom, then the total fluorescent cross section σ_f would be the same as the absorption cross section. However, the photon may suffer a collision with an electron in an outer shell and be absorbed with the ejection of a second electron from the atom (an Auger electron) and emission of an L , M , etc., X-ray photon (see Figure 1). The probability of this occurrence (called the fluorescent yield) is expressed as ϵ , so that (to first approximation) the cross section for fluorescence σ_f is given by

$$\sigma_f = \epsilon \sigma_{\alpha} \quad (2)$$

The factor ϵ can be quite small for the lower Z elements.

The attenuation of an X-ray beam of energy E_i through a material of constant Z can be expressed by Beer's law,

$$\ln \tau_{E_i} = \ln(I/I^0)_{E_i} = - \int_0^L \sigma_{\alpha} n(x) dx \quad (3)$$

where n is the number density of atoms, which may vary along the path x , and L is the total thickness of the material. The number $Q_{K_{\alpha}}$ of fluorescent K_{α} photons emitted at a distance x_0 along the path, from the monochromatic beam of volume dV into a solid angle $d\Omega$, is accordingly

$$Q_{K_{\alpha}} = I^0 [\exp(- \int_0^{x_0} \sigma_{\alpha} n(x) dx)] (\epsilon \sigma_{\alpha})_{E_i K_{\alpha}} n(x_0) dV \frac{d\Omega}{4\pi} \quad (4)$$

where x_0 is the location along the path at which the measurement is made and I^0 is the incident flux X-ray photons. Similar expressions describe the emission rate of other characteristic photons (K_β , L_α , etc.) due to excitation by a beam of E_i photons.

We now ask, "How can the principles of Equations (3) and (4) be used to extract information from gas/particle flow fields?"

2.2 Application.

Consider a gas/particle flow that is cylindrically symmetric and contains several atomic species. A typical solid propellant exhaust will provide an illustrative gas/particle flow. A 15 percent aluminized propellant rocket having a 5-cm dia exit nozzle is chosen as typical of tactical missile rockets or test models. Table 1 gives the computed one-dimensional equilibrium exhaust species composition for this rocket motor, which will be used for feasibility calculations.⁹

Three measurement possibilities from an incident X-ray beam are considered:

- a. Absorption at selected wavelengths
- b. Average fluorescence from a small volume at selected wavelengths
- c. Instantaneous fluorescence at selected wavelengths from events when individual particles cross the X-ray beam.

The information to be gained from each of these measurements and the problems that can be foreseen will be outlined briefly in the following paragraphs.

9. Gordon, S. and McBride, B. I., "Computer Program for Calculation of Complex Chemical Equilibrium Composition, Rocket Performance, Incident and Reflected Shocks, and Chapman-Hougenet Detonations." NASA Lewis Research Center, NASA-SP-273, 1971.

TABLE 1. MOLE FRACTION OF NOZZLE EXHAUST PRODUCTS FOR TYPICAL ALUMINIZED SOLID PROPELLANT ($p = 1 \text{ atm}$, $T = 1291^\circ\text{K}$).

<u>MOLECULAR SPECIES</u>	<u>MOLE FRACTION</u>
H_2	0.376
CO	0.258
HCl	0.120
$\text{Al}_2\text{O}_3 \text{ (solid)*}$	0.0970
N_2	0.0693
H_2O	0.0640
CO_2	0.0097
H	0.0036
Cl	0.0011
KCl	0.0002

* Assumed to be $1 \mu\text{m}$ particles.

2.2.1 Absorption.

The Beer's law expression, Equation (3), for the absorption of X-ray photons at an incident energy, E_i , by the mixture of elemental species j in the rocket flow at some position y from the flow axis (see Figure 3) is expressed

$$\ln \tau_{E_i}(y) = - \int_0^L \sum_j \sigma_j(E_i) n_j(x) dx \quad (5)$$

where the species densities may vary along the absorption path.

Note that for a circular symmetric flow configuration Equation (5) is in the form of an Abel integral, so that the local value of the kernel can be obtained by inversion;¹⁰ that is,

$$\sum_j \sigma_j(E_i) n_j(r) = - \frac{1}{\pi} \int_r^R \frac{\frac{d}{dy} [\ln \tau_{E_i}(y)]}{\sqrt{r^2 - y^2}} dy \quad (6)$$

Equation (6) can be expressed as a linear transformation matrix equation

$$\bar{S} N = T \quad (7)$$

where \bar{S} is an $i \times j$ matrix with elements σ_{ij} , N is a j dimensional density vector with density elements n_j , and T is an i dimensional measured transmittance vector with elements t_i corresponding to different values of the incident photon energy, E_i and defined by the integral on the right side of Equation (1). Inversion of Equation (7) yields the n_j elemental densities. If some of the $\sigma_{ij} n_j$ products are negligible with respect to others, the problem simplifies considerably.

In order to determine if such measurements of transmission are feasible, consider a homogeneous path. The n_j of Equation (5) are no longer functions of x and, for a path length L ,

10. Griem, H. R., Plasma Spectroscopy, McGraw-Hill Book Co., New York, 1964, pp. 176-178.

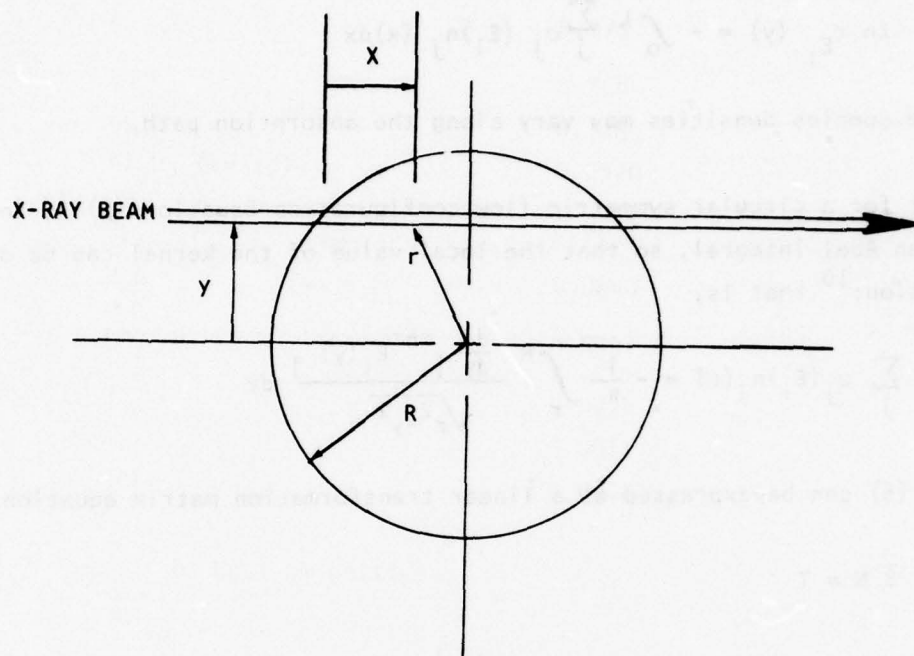


Figure 3. Orientation of X-Ray Absorption Path with Combustion Medium.

$$\ln \tau_{E_i} = - \sum_j \sigma_j(E_i) n_j L \quad (8)$$

and the elements t_i of Equation (7) become

$$t_i = - \frac{\ln \tau_{E_i}}{L} \quad (9)$$

The elemental density in the exhaust of the typical rocket exhaust described above is given in Table 2, along with the X-ray properties¹¹ of the different atoms present. From the standpoint of X-ray absorption or fluorescence, hydrogen can be neglected because of its low cross section, and potassium because of its low concentration. The absorption cross sections¹¹ of the remaining five elements (carbon, nitrogen, oxygen, aluminum, and chlorine) are plotted as a function of incident photon energy in Figure 4.

The following assignments of subscripts j for the elements and i for measurement energies are made:

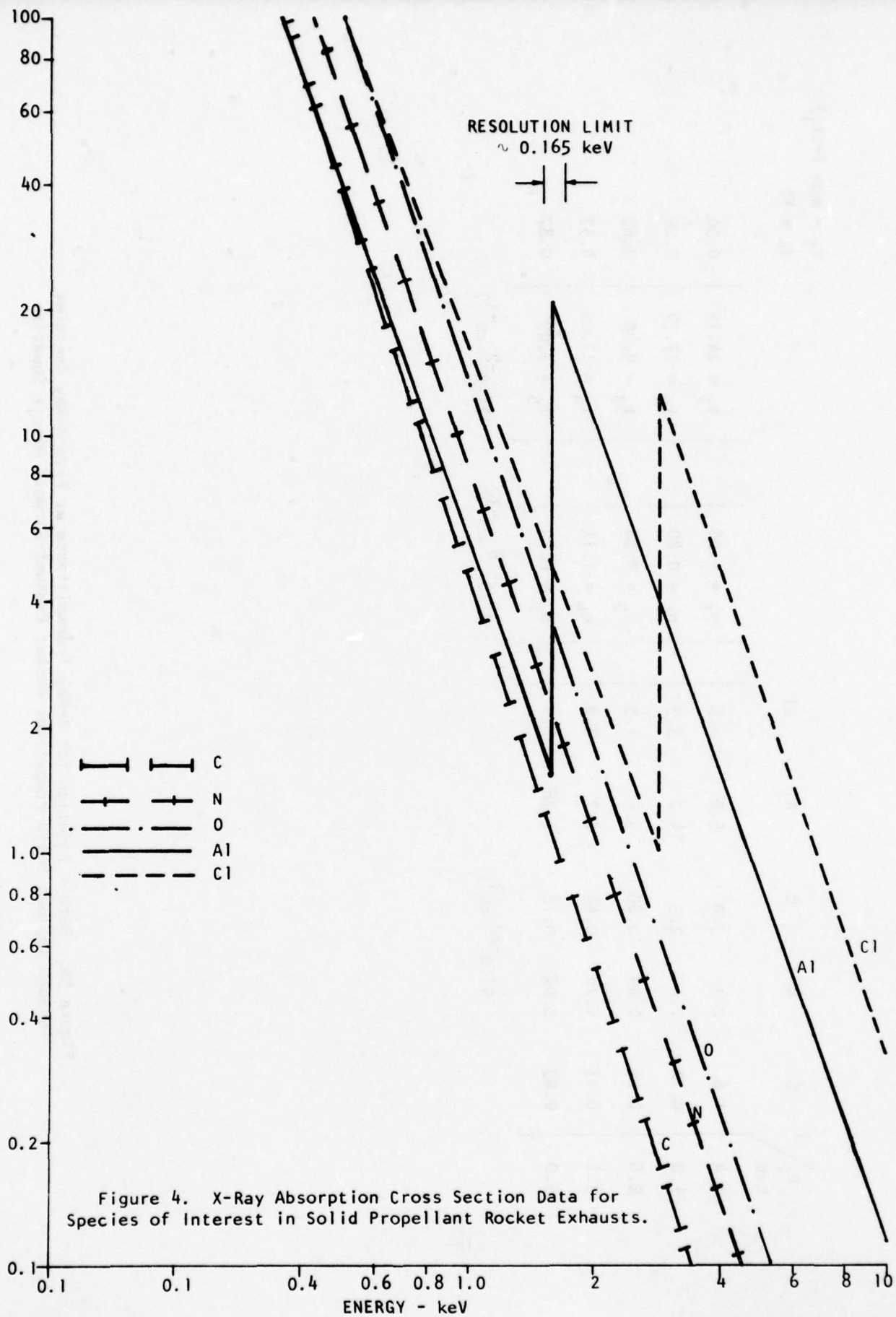
ELEMENT	j	ENERGY(keV)	i
C	1	1.4	1
N	2	1.8	2
O	3	2.6	3
Al	4	3.2	4
Cl	5	5.0	5

The matrix, Equation (7), can then be written out as shown on Figure 5a. The transmittance for each energy is also shown for the $L=5$ cm path length. Clearly, the τ_i at the energies chosen are measurable. Furthermore, the matrix S can be inverted so that all five species densities are determinate. The inverse matrix \bar{S}^{-1} is also given in Figure 5b. The individual species'

11. Brown, W. D. "X-Ray Attenuation and Absorption Coefficients," The Boeing Co. Report No. D2-125065-1, Sep 1966.

TABLE 2. ATOMIC SPECIES DENSITIES AND X-RAY PROPERTIES FOR SPECIES CONTAINED IN
TYPICAL ALUMINIZED PROPELLANT ROCKET EXHAUST.

ATOMIC SPECIES	NUMBER DENSITY (10^{18} cm^{-3})	K α ABSORPTION EDGE ENERGY (keV)	K α CHARACTERISTIC LINE ENERGY (keV)	ABS. CROSS SECTION AT A1 K α EDGE ($10^{-20} \text{ cm}^2/\text{atom}$)	FLUORESCENT YIELD FACTOR
H	5.78	0.0136	-	-	-
C	1.55	0.283	0.282	1.1	0.002
N	0.80	0.399	0.392	2.3	0.004
O	3.28	0.531	0.532	3.4	0.006
Al	1.12	1.559	1.486	20.6	0.036
Cl	0.70	2.819	2.621	5.0	0.094
K	10^{-3}	3.607	3.310	?	?



E_i keV	j	C	N	O	Al	Cl	$n_1 = 1.55$ $n_2 = 0.80$ $n_3 = 3.28$ $n_4 = 1.12$ $n_5 = 0.70$	$t_1 = 24.15$ $t_2 = 27.77$ $t_3 = 9.90$ $t_4 = 11.05$ $t_5 = 3.09$	$\tau_i = \exp(-Lt_i)$ (L = 5)
1.4		1.6	2.1	3.0	5.0	1.5			0.30
1.8		0.72	1.4	2.3	14.0	3.3			0.26
2.6		0.24	0.49	0.80	5.0	1.3			0.62
3.2		0.13	0.28	0.44	2.7	8.8			0.57
5.0		0.05	0.08	0.12	0.78	2.4			0.87
							$N(10^{-18} \text{ cm}^{-3})$	$T(10^{-2} \text{ cm}^{-1})$	

n_1	n_2	n_3	n_4	n_5	t_1	t_2	t_3	t_4	t_5
-0.2430	+1.6240	-0.5780	-0.0544	-0.0025	+14.6500	-55.0300	+31.0500	- 0.2960	+ 0.0733
-12.890	-12.830	+17.040	- 0.885	+ 3.2280	- 41.66	+153.900	- 86.720	+ 1.059	- 0.272
+50.3400	+34.9100	-56.6400		- 0.0129					

$N(10^{18}\text{cm}^{-3})$	$T(10^{-2}\text{cm}^{-1})$	$S^{-1}(10^{20}\text{cm}^{-2})$
n_1	t_1	- 0.2430
n_2	t_2	+1.6240
n_3	t_3	-0.5780
n_4	t_4	-0.0544
n_5	t_5	-0.0025

Figure 5b. Matrix Equation for X-Ray Transmittance at Five X-Ray Energies Through Typical Solid Propellant Rocket Exhaust-Inverse Matrix Equation

contributions to the transmittance (absorption) are shown in the array of Figure 6. From these calculations it is obvious that accounting for all five of the species must be considered in the inversion of the t_i to n_i .

In a thorough study of the feasibility of the technique, a sensitivity of the matrix inversion to errors in cross sections and transmittance measurements should be made. In this limited study, the sensitivity of the transmittance to 10 percent changes in the elemental densities should give an indication of the sensitivity. The results for 10 percent changes in Al and Cl densities are as follows:

E_i	$\pm 10\% n_4(\text{Al})$			$\pm 10\% n_5(\text{Cl})$		
	-	0	t_i +	-	0	t_i +
1.4	.307	0.300	0.291	0.306	0.300	0.292
1.8	0.273	0.255	0.234	0.258	0.255	0.252
2.6	0.630	0.617	0.597	0.617	0.617	0.611
3.2	0.581	0.572	0.564	0.594	0.572	0.559
5.0	0.867	0.866	0.859	0.872	0.866	0.857

The conclusion to be drawn from this exercise is that a 10 percent change in either Al or Cl results in only a small change (2 percent at the most) in the transmittance. Similar changes in O, N, and C densities produced even less changes in transmittance. Hence, 10 percent change in atomic density would be about the limit of sensitivity of the absorption technique as configured here. However, the energy choices were made quite arbitrarily, keeping in mind only that they should lie on either side of absorption edges, that five values should be used in order to invert the transmittance matrix and determine individual species concentrations, and that an energy detection resolution of about 0.2 keV is a practical choice for energy dispersive detection systems. Optimization of energy values used for detection and other sensitivity enhancement procedures requires further study.

$\frac{E_j}{E_i}$ (keV)	1	2	3	4	5	$\tau_i = \pi_j \tau_{ij}$
	C	N	O	Al	Cl	
1.4	0.88 (.12)	0.92 (.08)	0.61 (0.39)	0.76 (0.24)	0.80 (0.20)	0.30
1.8	0.95 (0.05)	0.95 (0.05)	0.69 (0.31)	0.46 (0.54)	0.89 (0.11)	0.26
2.6	0.98 (.02)	0.98 (0.02)	0.88 (0.12)	0.76 (0.24)	0.96 (0.04)	0.62
3.2	0.99 (0.01)	0.99 (0.01)	0.93 (0.07)	0.86 (0.14)	0.73 (0.27)	0.56
5.0	0.996 (0.004)	0.997 (0.003)	0.98 (0.02)	0.96 (0.04)	0.92 (0.08)	0.87

τ_{ij}
(α_{ij})

Figure 6. X-Ray Transmittance Array for Species of Interest in Solid Propellant Rocket Exhausts at Five Values of Energy

The geometrical integral inversion to obtain local elemental densities, Equation (6), suffers from the same propagation uncertainty problems of all such inversions.¹² However, the problems have been adequately addressed in the literature and are certainly no worse for X-ray absorption than spectral line emission or absorption in the UV-Vis-IR. It should also be noted that the analysis conducted here did not consider other refinements such as the influence of the spectral structure of the detector resolution band or the variation of the absorption cross sections over the resolution band. Such effects should not alter the basic conclusions of the study.

2.2.2 Mean Fluorescence.

The concept for measurement of the rate of emission of fluorescent photons excited by an X-ray beam passing through a medium containing a mixture of j species is illustrated in Figure 7. The path is assumed to be broken up into a number of elements of length Δx_k , where the index k designates the location of the field of view of a designated detector along the X-ray beam. The incident flux rate of the X-ray beam per unit energy at any give energy, E_i , will be attenuated as it passes through the medium so that at a position k the flux $I_k(E_i)$ at energy E_i is given by

$$I_k(E_i) = I^0(E_i) \exp\left(-\sum_k \sum_j \sigma_{ij} n_{jk} \Delta x_k\right) \quad (10)$$

where $I_k^0(E_i)$ is the incident flux and n_{jk} is the density of atoms of species j at the position k . The number of fluorescent K_α photons emitted by species j from a volume dV located at position k due to all the incident photons with energy greater than the K_α energy ($E_i > E_j$) into a solid angle $\Delta\Omega$ will be

12. Shelby, R. T. and Limbaugh, C. C., "Smoothing Technique and Variance Propagation for Abel Inversion of Scattered Data," AEDC-TR-76-163, Arnold Air Force Station, TN, 1976.

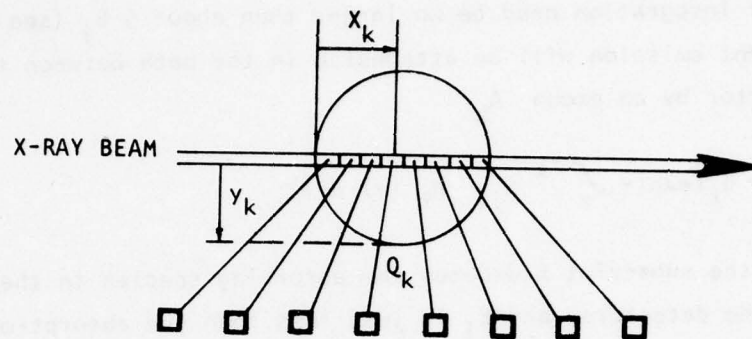


Figure 7. Concept of X-Ray Fluorescence Measurements for Combustion Flow Diagnostics.

given by

$$Q_{jk}(K_{\alpha}) = \int_{E_j}^{\infty} I_k(E_i) (\epsilon_j \sigma_{ij}) n_{jk} \Delta V \frac{\Delta \Omega}{4\pi} dE_i \quad (11)$$

The absorption cross section decreases quite rapidly with energy E_i so that the upper limit of integration need be no larger than about $5 E_j$ (see Figure 4). The fluorescent emission will be attenuated in the path between the beam and the detector by an amount A_k

$$A_k(E_j) = \Pi_{\ell} \{ \exp[- \int_0^{y_k} \sigma_{j\ell} n_{\ell}(y) dy] \} \quad (12)$$

In Equation (12), the subscript ℓ denotes the absorbing species in the path from the beam to the detectors, and E_j is just less than the absorption edge energy, so that σ_{jj} is the cross section for E_j fluorescent photons at the bottom of the absorption edge. Finally, the number of K_{α} photons arising from the viewing zone k emitted by species j which reach the detector is given by

$$q_{jk}(K_{\alpha}) = A_k(E_j) Q_{jk}(K_{\alpha}) \quad (13)$$

For the rocket flow field at hand $q_{jk}(K_{\alpha})$ can be determined for Al K_{α} and Cl K_{α} lines if some form of $I^{\circ}(E_i)$ is assumed. A convenient assumption is that $I^{\circ}(E_i)$ is a constant over the energy range of interest (1 to 10 keV).

It is also expeditious for purposes of calculation to express the absorption cross sections of Figure 4 in mathematical form; that is, with σ_{ij} expressed in units of Barns (10^{-20} cm^2) per atom,

Carbon	$\sigma_{ij} = 4.54 E_i^{-3.18}$	$E_i > 0.283 \text{ keV}$
Nitrogen	$\sigma_{ij} = 8.09 E_i^{-2.91}$	$E_i > 0.299 \text{ keV}$
Oxygen	$\sigma_{ij} = 13.2 E_i^{-2.92}$	$E_i > 0.531 \text{ keV}$
Aluminum	$\sigma_{ij} = 5.51 E_i^{-2.89}$	$1.559 > E_i > .087 \text{ keV}$
	$\sigma_{ij} = 77.4 E_i^{-2.85}$	$E_i > 1.559 \text{ keV}$
Chlorine	$\sigma_{ij} = 15.5 E_i^{-2.64}$	$2.819 > E_i > 0.238 \text{ keV}$
	$\sigma_{ij} = 259.5 E_i^{-2.92}$	$E_i > 2.819 \text{ keV}$

Now, if the position k is chosen at the centerline of the combustion flow and the data of Table 2 and Figure 4 are used in Equations (10) through (13), the result for the Al K_{α} line is

$$q_{Al K} = 2.46 \times 10^{-3} \Delta V \frac{\Delta \Omega}{4\pi} I^{\circ}(E_i) \quad (14)$$

Now, the detectability of $q_{Al K_{\alpha}}$ is dependent only upon the experimental configuration, the detector system characteristics, and the flux rate of the X-ray source. The result for the chlorine K_{α} line is

$$q_{Cl K_{\alpha}} = 8.46 \times 10^{-3} \Delta V \frac{\Delta \Omega}{4\pi} I^{\circ}(E_i) \quad (15)$$

Translation of Equations (14) and (15) into a determination of feasibility must await further implementation consideration, e.g., specification of ΔV , $\Delta \Omega$, and $I^{\circ}(E_i)$.

The fluorescent technique has one advantage over the absorption technique which is immediately obvious. The number of emitted K_{α} photons from a species is directly proportional to the number density of that species so that, except for the attenuation effects, a 10 percent change in n_{jk} causes almost a 10 percent change in q_{jk} ; the attenuation amounts to only about a 1 percent effect. Furthermore, the fluorescent technique gives a localized measurement of species concentration, avoiding the horrendous inversion problem and the necessity for assuming cylindrical symmetry. On the other hand, the absorption technique provides the opportunity to measure densities of all the absorbing species in the flow whether an amenable absorption edge is present or not. The greatest advantage of the absorption technique seems to be that the measurement itself is less difficult.

2.2.3 Particle Fluorescence.

If a very small X-ray beam is passed through a gas/particle flow and particles containing atomic species j with sizes smaller than the beam diameter pass through the beam one at a time, then a K_{α} fluorescent event occurs such that

the maximum rate of K_α photons emitted will be

$$q_{jk}(t) = \int_{E_j}^{\infty} I_k(E_i) (\epsilon_j \sigma_{ij}) N_j A(E_j) dE_i \quad (16)$$

where N_j is the total number of j atoms in the particle and $A(E_j)$ is the transmittance along the path to the detector. If the beam diameter is δ and the particle diameter is d and $d < \delta$, then the pulse shape will be similar to the illustration of Figure 8. The total number of j atoms in the particle can be determined from Equation (12), where $I_k(E_i)$ and $A_k(E_j)$ are given by Equations (10) and (12), respectively. For Al_2O_3 particles $1 \mu m$ in dia (1.6×10^{10} Al atoms per particle) and with the gas/particle and X-ray properties of Table 2 and Figure 4, the maximum photon rate reaching the detector from the stream axis for a single scattering event will be about

$$q_{jk}(Al K_\alpha) = 4 \times 10^{-11} \text{ } 1^\circ \quad (17)$$

The total number of counts will be

$$Q(Al K_\alpha) = \int q_{jk}(t) dt = 4 \times 10^{-11} \text{ } 1^\circ \Delta t \quad (18)$$

where Δt is the time required for the particle to pass through the beam. Velocities in rocket exhausts are about 2×10^5 cm/sec so that for a 1 mm beam, $\Delta t \approx 0.5 \times 10^{-6}$ sec. Thus, 1° must be on the order of 10^{19} photons/cm² sec in order to produce about 100 counts during an event.

If the X-ray beam is rectangular with width δ along the flow axis and with a dimension along the normal to the flow axis large with respect to the particle diameter d (spherical particles are assumed here), then the fluorescent photon pulse shape may be depicted as in Figure 8. Now, note that two time increments can be identified, the rise time $\Delta t'$ and the total duration of the pulse, Δt . Furthermore,

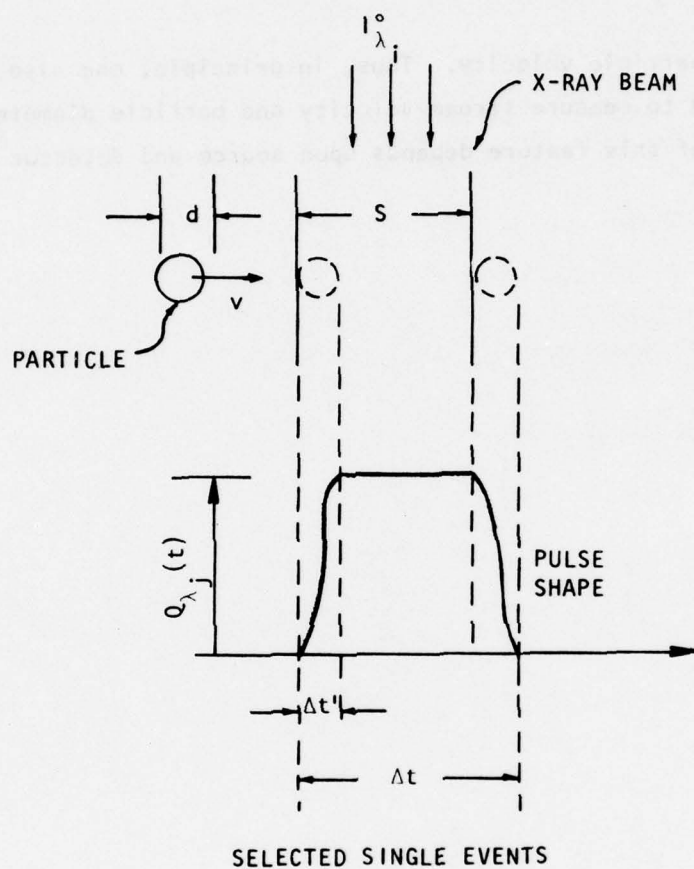


Figure 8. Scattering Event Chronology for a Particle Passing Through an X-Ray Beam.

$$\Delta t' = \frac{d}{v} \quad (19)$$

$$\Delta t = \frac{\delta + 2d}{V} = \frac{\delta}{V} + 2\Delta t' \quad (20)$$

where V is the particle velocity. Thus, in principle, one also has a potential method to measure stream velocity and particle diameter. Again, implementation of this feature depends upon source and detector performance.

3. IMPLEMENTATION CONSIDERATIONS.

3.1 System Description.

An elementary description of a modern energy dispersive X-ray system which might be used for the gas/particle diagnostics application is given in this section. The purpose is to identify the most important properties of such a system and not to present a comprehensive treatise on the subject. The latter can be much better accomplished by reference to a text on the subject of X-ray energy spectroscopy.⁸

The basic components of an X-ray absorption or fluorescence system suitable for making measurements in gas/particle flows are a source and a detector system. The source is provided by an electron gun capable of focusing a high flux of electrons on a target which emits the X-rays. One configuration is shown schematically in Figure 9. The voltage applied, the target material, and the target configuration determine the energy spectrum and flux produced by a particular source. A relative spectrum which might be expected from a chromium target is shown in Figure 10 for different values of the electron energy. The continuous portion of the spectrum is produced by free electron-electron encounters while the characteristic lines are produced by the fluorescence process discussed in Section 2.

The design problem for the application under consideration here is to produce a high intensity, collimated beam of 1 to 10 keV X-ray photons. The photons are not isotropically emitted so that the intensity to be expected at some distance R and angle θ from the target is given by

$$I^o(E_i) = Y(E_i, \theta) q_e / 4\pi R^2 \quad (21)$$

where q_e is the electron current and $Y(E_i, \theta)$ is a photon emission efficiency factor for the particular target material and geometry.

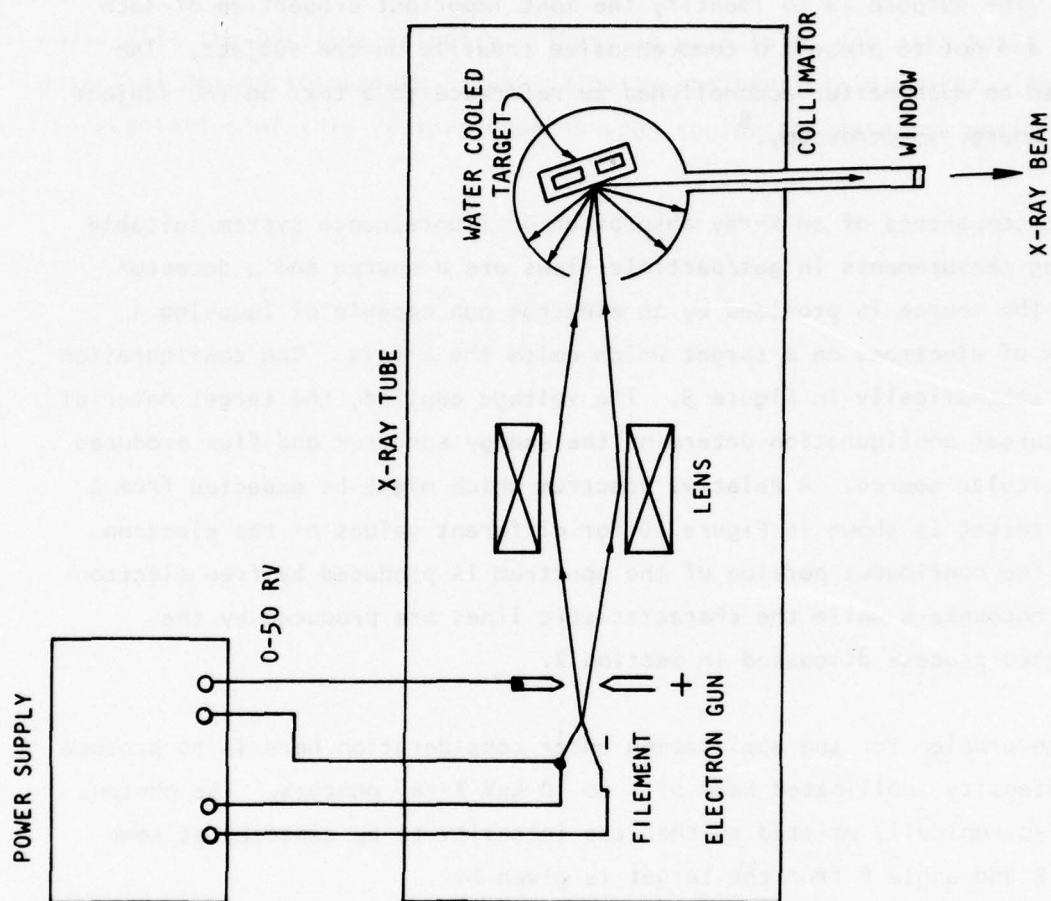


Figure 9. Schematic of X-Ray Beam Source.

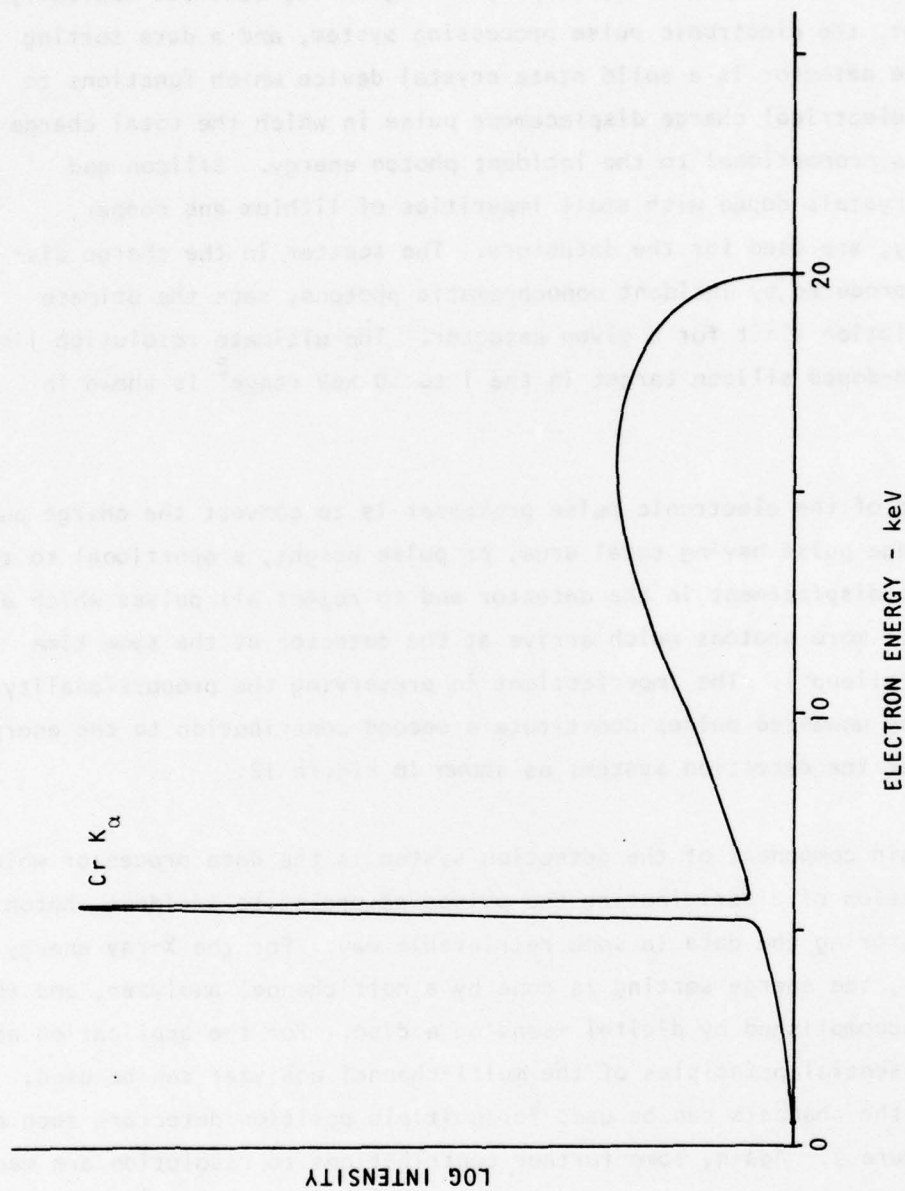


Figure 10. Approximate X-Ray Energy Spectrum from Chromium Target.

The detector system, shown schematically in Figure 11, consists basically of the detector, the electronic pulse processing system, and a data sorting system. The detector is a solid state crystal device which functions to produce an electrical charge displacement pulse in which the total charge displaced is proportional to the incident photon energy. Silicon and germanium crystals doped with small impurities of lithium and copper, respectively, are used for the detectors. The scatter in the charge displacement, produced by incident monochromatic photons, sets the ultimate energy resolution limit for a given detector. The ultimate resolution limit of a lithium-doped silicon target in the 1 to 10 keV range⁸ is shown in Figure 12.

The function of the electronic pulse processor is to convert the charge pulse into a voltage pulse having total area, or pulse height, proportional to the total charge displacement in the detector and to reject all pulses which are due to two or more photons which arrive at the detector at the same time (so called "pileup"). The imperfections in preserving the proportionality and rejecting unwanted pulses constitute a second contribution to the energy resolution of the detection system, as shown in Figure 12.

The third main component of the detection system is the data processor which has the function of discriminating the pulses according to incident photon energy and storing the data in some retrievable way. For the X-ray energy spectrometer, the energy sorting is done by a multichannel analyzer, and the storage is accomplished by digital means on a disc. For the application at hand, the essential principles of the multi-channel analyzer can be used, but some of the channels can be used for multiple position detectors such as shown in Figure 7. Again, some further contributions to resolution are made by the data processing step.

Typical commercial detection systems have an energy resolution of from 0.15 to 0.2 keV, as illustrated in Figure 12. The effect of resolution on sensitivity for the diagnostics problem is a subject requiring further study.

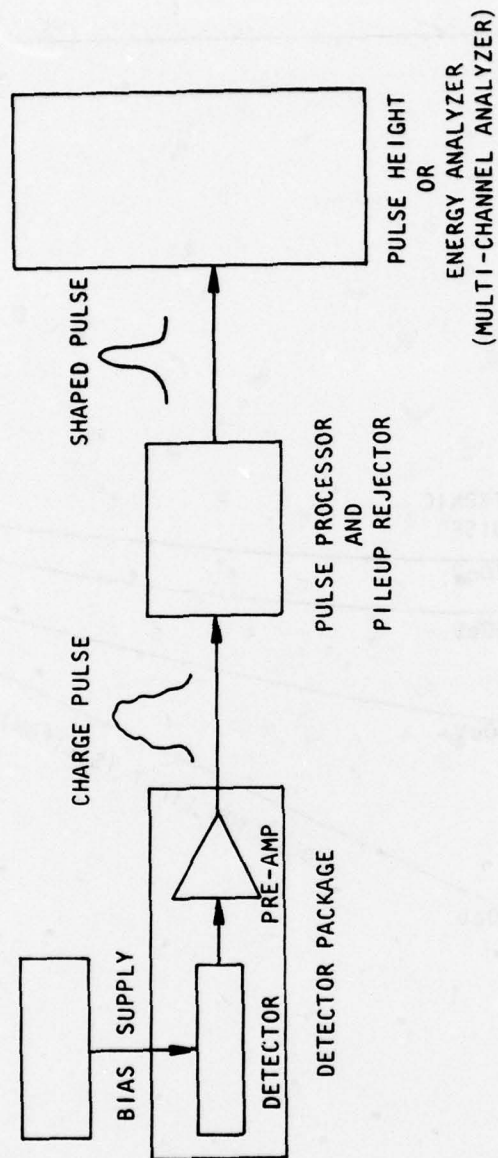


Figure 11. Functional Diagram of Energy Dispersive X-Ray Detection System.

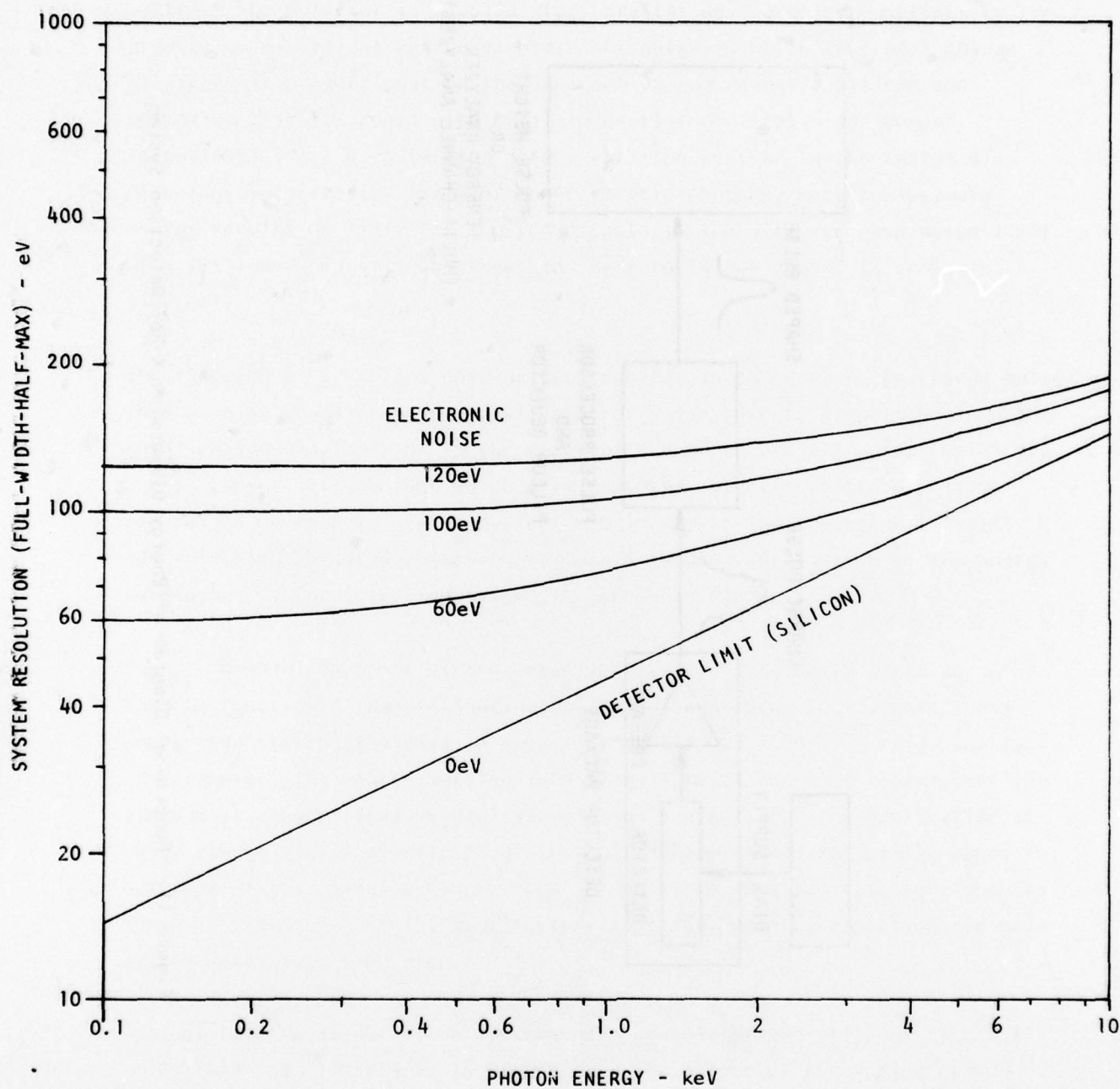


Figure 12. Detector and Electronic Contributions to System Resolution⁸

8. Woldseth, R., X-Ray Energy Spectrometry, published by Kevex Corp., Burlingame, CA, 1973.

3.2 System Performance Criteria.

Typical commercially available detector systems are capable of about 50,000 counts per second with corrections automatically applied for pileup rejection and dead time and with an energy resolution of about 0.165 keV for a detector with an area of 80 mm^2 . Good instrumentation practice demands about 100 data points per time resolution element. For the rocket application about 0.1 sec temporal resolution is desired. Hence, the data rate in each channel must be at least 1,000 per second. The two measurements, absorption and fluorescence, place different requirements on the detector system. For the absorption case the problem is that too many photons arrive at the detector per second in the entire energy range of the source. Thus, the source must be filtered to eliminate photons with energy larger than the region of interest (about 8 to 10 keV), and the intensity controlled so that the total incident photon rate within the energy spectrum is less than the maximum count rate of the detector system. One method of controlling the count rate is by controlling the beam size or detector aperture. Note that the absorption measurement requires that a detector with a small area be provided for good spatial resolution. Furthermore, it would be nice if the measured intensity $I(E_i)$ were nearly constant across the energy range of interest. This would require that $I^\circ(E_i)$ be an increasing function of E_i . Further tailoring of the intensity dependence on energy is left to the experimental follow-on of this work.

The fluorescence detection problem is likely to be one of insufficient photon count rate rather than too high a photon count rate. Referring to Equations (14) and (15) and assuming a 1 mm dia beam, a view resolution of 5 mm along the beam, and a detector area of 80 mm^2 with the detector located about 30 cm from the beam, the requirement for 1,000 counts per second results in a beam intensity of about 10^{11} photons/sec cm^2 for the Al K_α lines and about 3×10^{10} photons/sec cm^2 for the Cl K_α lines. Of course, in the derivation of Equations (14) and (15) a constant intensity with energy was assumed. Also, note that the fluorescence detection rate can be increased by either increasing the beam diameter or increasing the detector area, both of which are in conflict with the absorption requirement.

The diagnostics concept outlined in Section 2.2 required both absorption and fluorescence measurements since it is necessary to correct the fluorescence count for both beam attenuation and path attenuation. Thus the final design of a single system must meet the conflicting requirements of the absorption and fluorescence measurements. High intensity, large beam diameter, and a large area detector are required for the fluorescence measurement. A small beam diameter, much lower intensity, and a small area detector are required for the absorption measurement. These requirements can be met in a single system by providing the high intensity source with large beam size and controlling the intensity reaching the absorption detector by filtering at that point, as well as providing an adjustable aperture in front of the absorption detector.

4. DISCUSSION.

4.1 Laboratory Demonstration Experiments.

The feasibility analysis of Section 3 has served to indicate that measurements of X-ray absorption and fluorescence on rocket exhaust flows may yield elemental density distributions in the flow. The measurements appear to be practically feasible, and the data analysis appears to be tractable. However, no technique can be placed on sound footing without a thorough laboratory investigation. Furthermore, a sufficient number of questions were raised regarding sensitivity, propagation of errors, source energy distribution tailoring, selection of measurement wavelengths, etc., to warrant a rather extensive laboratory investigation. Such an investigation must include, in addition to the examination of the above mentioned questions, the following:

Identification and specification of equipment

Safety procedures

Development of a well-defined, quantified laboratory gas/particle flow system

Design of experiments to clearly demonstrate proof of the principles involved

Development of measurement methodology

Identification of and solutions for the problems to be encountered in field application (path attenuation, equipment protection, etc.)

4.2 Concept of a Typical Rocket Test Application.¹³

It may be instructive to examine the question of how an X-ray diagnostic would be used in a rocket propulsion development program. One of the

13. The concept of the rocket test scenario is a result of discussions between the author and his colleagues, Mr. Jay Levine and Dr. Dave Mann, during the course of this study.

principal contributors to performance losses in rocket motors is the momentum and energy losses imposed by particles in the flow. The losses in thrust occur because the particle drag does not permit the particulate mass to follow the expansion of the gas flow field and because the particles do not convert inherent thermal energy into velocity as the gas expands. The current knowledge about this phenomena is limited to experience gained through theoretical models of the gas-particle drag interaction and gas/particle heat transfer in which assumptions of particle shape, density, emissivity, physical state, and size distributions are made. In the past, the specific assumptions made for aluminized propellant motors are that the Al_2O_3 particles are spherical in shape, that the state (liquid or solid) is controlled by the temperature, that the particles have the density of solid or liquid Al_2O_3 , and that an initial assumed size distribution at the entrance to the contraction section of the nozzle does not change throughout the nozzle flow process. Empiricism is built into the model by adjustment of the particle size distribution to fit experimentally measured performance for a few select cases. Modeling efforts now underway include many refinements of the gas/particle interaction, but guidance is lacking as to the effects produced by the refined treatments.

The current status of rocket motor development is built around squeezing as much additional specific impulse out of a system as possible. Particle drag may account for as much as 30 to 10 percent loss in specific impulse. Theoretical studies indicate that drag losses increase rapidly with particle size. Thus, improvements in understanding the impact of the assumptions listed above becomes important. Experiments of a conventional nature in which only thrust and pressures are measured do not yield insight into the validity of the assumptions or the sensitivity of the performance to them. Thus, experiments in which some of the particle field properties are measured directly is sought.

A preliminary conception of an experiment leading to advancement in fundamental knowledge of the gas/particle flow process is described as follows:

Objective: To provide a set of gas/particle flow measurements that can be used to better understand two-phase flow losses and to examine the validity of the assumptions made about particle properties in rocket motor performance modeling.

Experiment Plan: Fire identical, aluminized propellant rocket motors with several lengths of conical nozzles (Figure 13). Measure, in addition to thrust, chamber pressure, and nozzle wall static pressures, the elemental mass (atomic density) distribution of Al and Cl as a function of radius at the nozzle exit available for the several expansion ratios using the X-ray spectroscopic technique, and utilize other available techniques to determine gas and/or particle temperature, species densities, or particle sizes.

Analysis: Exercise the analytical model to predict nozzle exit radial and axial distribution of particulate mass and nozzle-wall static pressure distribution, iterating on the various particle properties until as close a fit as possible of the various measurements is achieved.

Result: New insight into particle properties and flow behavior in rocket nozzle flows, leading to more accurate modeling of solid propellant rocket motors.

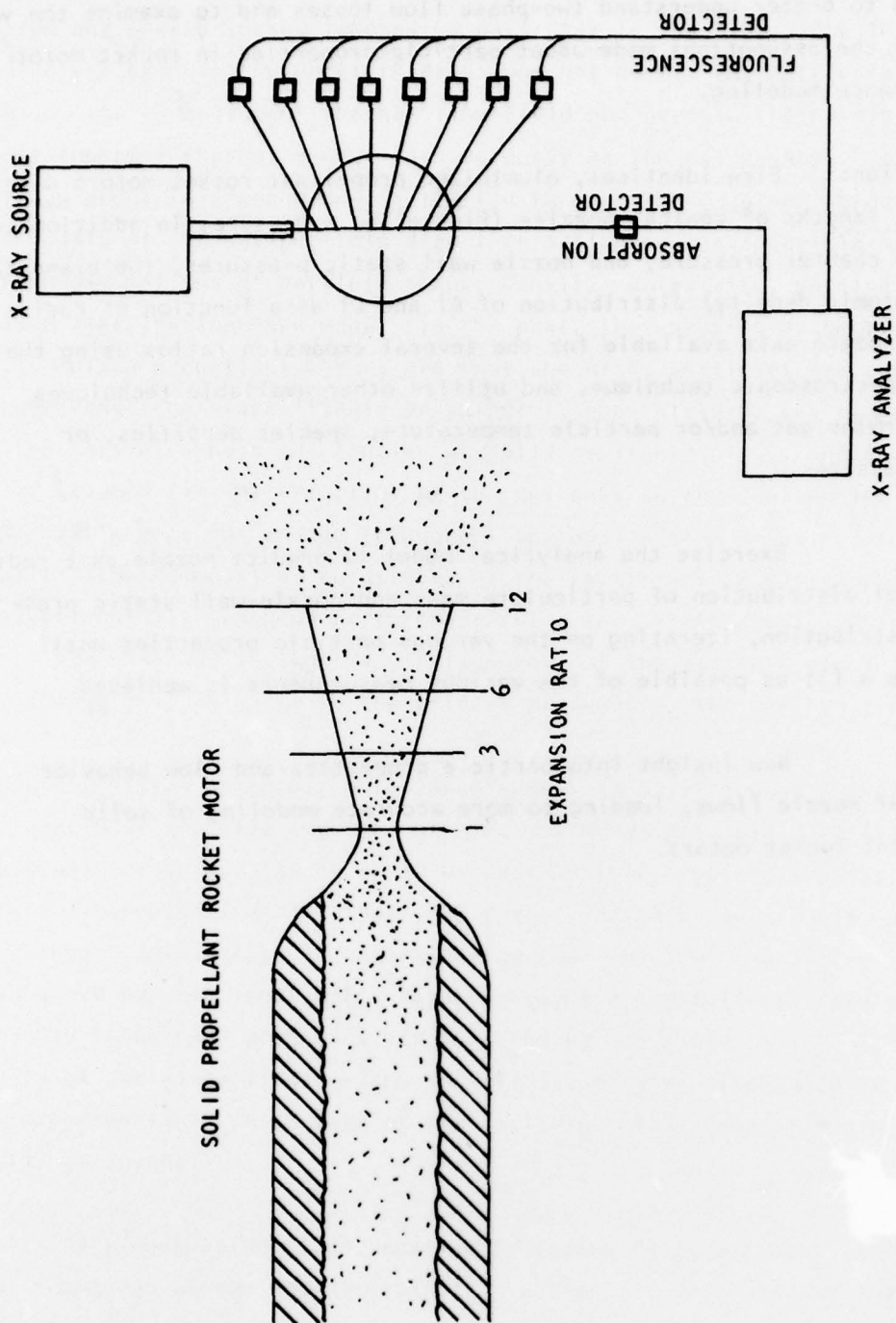


Figure 13. Concept of X-Ray Measurement of Elemental Concentration at Exhaust Plane of Solid Propellant Rocket Motors.

4.3 Future Directions.

The preliminary analysis conducted here has shown that X-ray techniques are feasible (in principle) and the framework for follow-on work has been laid. It is highly desirable that the elemental densities be determinable from a first principal calculation. In order that this be done accurately, better accounting for the peculiarities of the source and detection apparatus must be made. Such an accounting would include incorporation into the equation of Section 2 the exact source intensity spectrum and the spectral shape of the detection system resolution window.

In the investigation reported here, no effort was made to obtain the most accurate cross section and fluorescent yield data. An accurate first principle calculation must, of course, begin with accurate X-ray property data. Thus an investigation of the accuracies of these parameters is necessary. Ordinary elemental analysis procedures rely on calibration of the various X-ray spectrometers using samples of known concentration. Moreover, laboratory analysis is almost always concerned with the relative concentrations of elements rather than absolute atomic densities, as required here. Hence, accurate cross section data is only of academic concern to the laboratory analyst and may not exist to the accuracy required for rocket flow diagnostics. One aspect of future work may therefore lie in conducting laboratory experiments to obtain more accurate cross section (both absorption and fluorescent) data.

It is also desirable to have a source spectrum tailored to optimize the sensitivity of the absorption and fluorescence measurements. cursory examination of the literature revealed a lack of reliable information on the relative intensity spectrum from various target materials as a function of the electron energy applied. One might visualize a target (see Figure 9) made of a combination of materials to selectively excite (or be absorbed by) a specific gas/particle mixture. For the application at hand, a source to efficiently excite Al and Cl is desired. For most efficient excitation the K_{α} radiation from elements lying just above Al and Cl in the periodic table

would be desirable. Thus, Si and P K_{α} radiation (1.74 and 2.02 keV, respectively) would excite Al K_{α} , and K and Ca K_{α} lines (3.31 and 3.69 keV, respectively) would be desirable for Cl. For the absorption measurement, such a source in which a large portion of the intensity is composed of very narrow spectral lines would be desirable in that the finite band width of the energy dispersive detection system would have less effect. For the fluorescence measurement the advantage would be more efficient excitation by having the incident intensity concentrated at an energy very close to the absorption edges of Al and Cl. It would appear that a laboratory investigation using an analytical type spectrometer could yield the information necessary to construct such targets.

An area of investigation relatively unexplored at this time is the interpretation of the high resolution fine structure around absorption edges and in fluorescence lines (so-called X-Ray Absorption Fine Structure, EXAFS).¹⁴ At resolutions of about 1 eV, such effects as crystalline structure (or lack thereof), bonding energy in molecules, isotope distribution, etc., contribute to the fine structure. One question which does not seem answerable from any diagnostic technique previously discussed is the physical state (liquid or solid) of the particles. If the fine structure of absorption edges or characteristic lines could be resolved, this determination might also be made. The technology for making such measurements is now in its infancy, but the potential as a diagnostic for the future should not be overlooked.

14. For example, see Citrin, P. H., "Principles of EXAFS Applied to Simple and Complex Systems," Paper EC-1, Bulletin American Physical Society, Vol. 22, March 1977, p. 359.

5. CONCLUSIONS AND RECOMMENDATIONS.

5.1 Conclusions.

The following conclusions can be drawn from the study presented herein:

- a. The transmittance of X-ray beams (in the 1 to 10 keV energy range) through the exhaust flow from a highly aluminized propellant; 1,000 lbf rocket ranges from 0.25 to 0.9, depending upon the X-ray energy and is therefore a feasible measurement. Interpretation of the measured transmittances in terms of local elemental densities is also feasible for the elements C, N, O, Al, and Cl, although sensitivity to changes of less than about 10 percent may impose problems. Further sensitivity analysis is required to optimize wavelength selection and X-ray source spectral characteristic.
- b. The mean rate of emission of characteristic (K_{α}) fluorescent lines of Al and Cl can be measured by commercially available detectors, provided source intensities of the order of 10^{12} photons/sec cm^2 are provided. Such sources are believed to be available using rotating electrode, electron gun type X-ray sources. Interpretation of the emitted K_{α} radiation in terms of local elemental density of Al and Cl is straightforward, but may require more accurate X-ray cross section and fluorescent yield factor data. Sensitivity of the fluorescent rate technique to changes in elemental concentration is about one to one. Again, optimization of implementation techniques is a key to success.
- c. Fluorescence bursts from a particle passing through an X-ray beam offers questionable feasibility at this time. Source intensities on the order of 10^{19} photons/sec cm^2 are required. The potential usefulness of such a diagnostic should not,

however, be overlooked, and additional investigation is therefore warranted.

5.2 Recommendations.

The feasibility study conducted was theoretical in nature and little experimental supporting evidence is available. Therefore, the following recommendations for future work are offered:

- a. Proof of principle experiments should be conducted in a laboratory environment. A recommended plan for the experiments was presented in 4.1.
- b. A rationale for rocket test environments should be developed using the experience gained in the proof of principle experiments, and a program, such as the "Particle Drag Loss" experiment described in 4.2, should be designed and implemented.
- c. Further exploratory studies to determine uncertainty limits and optimum equipment design should accompany or follow the proof of principle experiments. Such investigation may lead to the necessity for programs to obtain fundamental data on absorption cross sections, fluorescent yield factors, and electron bombarded target emission spectra.

REFERENCES

1. Goulard, R., Mellor, A. M., and Bilger, R. W., "Combustion Measurements in Air Breathing Propulsion Engines. Survey and Research Needs," Combustion Science and Technology, Volume 14, 1976, pages 195-219.
2. Self, S. A. and Kruger, C. H., "Diagnostic Methods in Combustion MHD Flows," Journal of Energy, Volume 1, 1977, pages 25-43.
3. "Applications of Non-Intrusive Instrumentation in Fluid Flow Research," AGARD CP-193, May 1976.
4. Zinn, B. T., Ed., "Experimental Diagnostics in Gas Phase Combustion Systems", Progress in Astronautics and Aeronautics, Volume 53, AIAA Press, 1977.
5. McGregor, W. K., "Assessment of In Situ Diagnostics for Application to Rocket Propulsion Problems," AFRPL-TR-78-62, (to be published).
6. Bertin, E. P., Principles and Practices of X-Ray Spectrometric Analysis, Plenum Press, New York, 1971.
7. Chun, J. W., "Quantitative Measurement of Aerosol Particulates with an Energy Dispersive X-Ray Spectrometer," NWC-TP-6012, Naval Weapons Center, China Lake, CA (to be published).
8. Woldseth, R., X-Ray Energy Spectrometry, published by Kevex Corp., Burlingame, CA, 1973.
9. Gordon, S. and McBride, B. I., "Computer Program for Calculation of Complex Chemical Equilibrium Composition, Rocket Performance, Incident and Reflected Shocks, and Chapman-Hougen Detonations." NASA Lewis Research Center, NASA-SP-273, 1971.
10. Griem, H. R., Plasma Spectroscopy, McGraw-Hill Book Co., New York, 1964, pages 176-178.
11. Brown, W. D., "X-Ray Attenuation and Absorption Coefficients," The Boeing Co. Report No. D2-125065-1, September 1966.
12. Shelby, R. T., and Limbaugh, C. C., "Smoothing Technique and Variance Propagation for Abel Inversion of Scattered Data," AEDC-TR-76-163, Arnold Air Force Station, TN, 1976.
13. The concept of the rocket test scenario is a result of discussions between the author and his colleagues, Mr. Jay Levine and Dr. Dave Mann, during the course of this study.
14. For example, see Citrin, P. H., "Principles of EXAFS Applied to Simple and Complex Systems," Paper EC-1, Bulletin American Physical Society, Volume 22, March 1977, page 359.